Self-trapping and oscillation of quadruple beams in high band gap of 2D photonic lattices

Shiqiang Xia (夏世强), Daohong Song (宋道红), Liqin Tang (唐莉勤)*, Cibo Lou (楼慈波), and Yigang Li (李乙钢)

The MOE Key Laboratory of Weak Light Nonlinear Photonics, TEDA Applied Physics School and School of Physics, Nankai University, Tianjin 300457, China

**Corresponding author: tanya@nankai.edu.cn*

Received March 14, 2013; accepted June 28, 2013; posted online September 3, 2013

Higher-band self-trapping and oscillation (rotation) of nonlinear quadruple beams in two-dimensional (2D) square photonic lattices are numerically demonstrated. Under appropriate conditions of nonlinearity, a quadruple-like beam can self-trap into localized modes that reside in the second Bragg reflection gap through single-site excitation. By changing the initial orientation of the incident quadruple beam related to the lattices, periodic oscillations of the localized quadruple mode may be obtained. The localized quadruple state becomes a rotating doubly charged optical vortex (DCV) during rotation and should undergo charge-flipping when the rotating direction is reversed.

OCIS codes: 080.1238, 190.4420, 050.4865.
doi: 10.3788/COL201311.090801.

Linear and non-linear light propagation in periodic photonic lattice has attracted strong research interest in recent years, and many fascinating light behaviors[1] have been demonstrated to contain a physical essence beyond optics, such as Anderson localization[2], Bloch oscillation, and Zener tunneling[3]. Photonic lattices serve as an ideal platform for exploring various fundamental issues in discrete systems, and exciting phenomena in new lattice settings, including super lattices[4], ionic-type photonic lattices[5], and three-dimensional photonic lattices[6,7], have been demonstrated. In a linear photonic lattice, light propagation is modulated in accordance with the Floquet-Bloch theorem[8]. The continuous spatial transmission spectrum is split into separate bands by forbidden gaps at the boundaries of the Brillouin zone due to Bragg reflections of the periodic potential. In the presence of appropriate nonlinearity, discrete diffractions can be balanced, with light self-trapping into localized states as lattice solitons. Many types of localized modes residing in different band gaps have been reported experimentally or theoretically in optically-induced photonic lattices on the basis of various band-gap structures, such as fundamental solitons[9], dipole solitons[10−13], vortex solitons[14,15], bandgap surface vortex solitons[16], higher-band vortex solitons[17], and embedded-soliton trains[18], to name only a few. Rotating properties of lattice solitons have also been demonstrated[19−23]. For instance, in optically induced periodic ring lattices, the soliton rotation in different lattice rings can be controlled by imposing an initial transverse momentum on the soliton[21]. Doubly charged vortices (DCVs)[22] and dipole solitons[23] have been reported to experience rotations in a square photonic lattice, which is especially interesting because the dipole soliton itself initially carries no angular momentum. Nevertheless, all of the solitons mentioned above are discrete solitons or gap solitons existing in the total internal reflection gap and the first Bragg reflection band gap. Therefore, whether or not a localized state residing in higher band gaps can be excited, as well as the dynamics of such excitation, must be investigated.

In this letter, we firstly calculate the dispersion relation (band structure) of two-dimensional (2D) square lattices and then determine the possibilities for localized quadruple states that reside in the second Bragg reflection band gap by inputting a quadruple-like beam through single-site excitation and investigating its rotational properties by analyzing its linear and nonlinear propagation in different orientations relative to the lattices.

Beam propagation through an optically induced photonic lattice in a biased photorefractive crystal is governed by the paraxial non-linear Schrödinger equation[24]:

$$\mathrm{i}\frac{\partial\psi}{\partial z}+D\left(\frac{\partial^2\psi}{\partial x^2}+\frac{\partial^2\psi}{\partial y^2}\right)-\frac{\gamma\psi}{1+I_{\mathrm{b}}(x,y)+\zeta|\psi|^2}=0, \tag{1}$$

where ψ is the slowly varying complex amplitude of the probe beam, $\zeta = 0, 1$ represent linear and nonlinear conditions, respectively, $I_{\mathrm{b}} = I_{\mathrm{g}}\{\cos[\pi(x+y)/d]+\cos[\pi(x-y)/d]\}^2$ is the lattice potential translated into a change in the refractive index Δn through the non-linearity in a photorefractive crystal, I_{g} is the lattice peak intensity in units of background irradiance, and $d = 23$ μm is the lattice spacing. The lattice is written in this fashion because it can be optically induced by interfering beams of ordinary polarization in experimental conditions. The probe beam is extraordinarily polarized along the crystalline c axis. The dimensionless variables x, y, and z are normalized to the typical scales $x_{\mathrm{s}} = y_{\mathrm{s}} = 1$ μm, and $z_{\mathrm{s}} = 1$ mm, respectively. The diffraction coefficient is $D = z_{\mathrm{s}}\lambda/4\pi n_{\mathrm{e}}x_{\mathrm{s}}^2$, $\gamma = 0.5k_0n_{\mathrm{e}}^3\gamma_{33}E_0z_{\mathrm{s}}$ is a nonlinear coefficient proportional to the electro-optic coefficient γ_{33} and the applied direct current (DC) field voltage E_0, and K_0 is the wave number. $n_{\mathrm{e}} = 2.35$ is the extraordinary refractive index of bulk photorefractive Strontium-Barium Niobate (SBN) crystal, and $\lambda = 532$ nm is the laser wavelength in vacuum. These parameters are selected so that they are consistent with a typical experimental setup[9,24−27].

The dispersion relation and Bloch modes for high-

symmetry points of such square photonic lattices are firstly studied. Light propagation in a periodic photonic lattice is characterized by the spatially-extended eigenmodes or Bloch waves[8]. Bloch waves are found as solutions of the linearized lattice equation, i.e., the linear form of Eq. (1) is

$$\mathrm{i}\frac{\partial\psi}{\partial z}+D\left(\frac{\partial^2\psi}{\partial x^2}+\frac{\partial^2\psi}{\partial y^2}\right)-\frac{\gamma\psi}{1+I_{\mathrm{b}}(x,y)}=0, \quad (2)$$

in the form $\psi=\mathrm{e}^{-\mathrm{i}\beta z}u(\mathbf{r})$, $\mathbf{r}=(x,y)$. Substituting this into Eq. (2), the eigenproblem can be obtained:

$$\beta u+D\left(\frac{\partial^2 u}{\partial x^2}+\frac{\partial^2 u}{\partial y^2}\right)-\frac{\gamma u}{1+I_{\mathrm{b}}(x,y)}=0, \quad (3)$$

$u(\mathbf{r};\mathbf{k})$ has the form $u(\mathbf{r};\mathbf{k})=\mathrm{e}^{\mathrm{i}\mathbf{k}\cdot\mathbf{r}}U(\mathbf{r};\mathbf{k})$, where $U(\mathbf{r};\mathbf{k})$ possesses the same periodicity as the lattice potential, $\mathbf{k}=(k_x,k_y)$ is the wave number, and $\beta(\mathbf{k})$ is the dispersion relation. Eigenproblem (3) can be solved numerically. For the square lattice shown in Fig. 1(a), $\beta(\mathbf{k})$ is depicted in Fig. 1(c), which is invariant with respect to the translation $k_{x,y}\rightarrow k_{x,y}\pm 2\pi/d$, and therefore fully defined by its values in the first Brillouin zone (Fig. 1(b)). Unlike the case of low lattice potential[24], a high lattice potential of $I_{\mathrm{g}}=1.50$ and a nonlinear coefficient of $\gamma=6.00$ (corresponding to $E_0=280$ V/mm) are selected so that the higher band gap can remain open. Figure 1(c) clearly shows that two complete gaps exist in this case. Bloch waves from different high-symmetry points of the first and second spectral bands have been previously discussed[24]. Here, calculated Bloch waves of the special high-symmetry points X and M in the third band, corresponding to the red points in Fig. 1(c), are shown; these waves will be used in the following discussion. Point M is located at the top of the third band, while point X is embedded in the band. Figures 1(d)–(g) show the intensities and corresponding phase structures. Figure 1(d) shows that Bloch waves have three intensity maxima centered between one lattice maximum for point X. Bloch waves originating from point M have four intensity maxima centered between the maximum of the square lattice (Fig. 1(f)), and the phase distribution resembles a chessboard for the four maxima (Fig. 1(g)).

Wave propagation in the square lattice is studied numerically by launching a beam with a quadruple structure:

$$U(x,y)=A\sum_{n=0}^{3}\mathrm{e}^{-\left[(x-x_n)^2+(y-y_n)^2\right]/r^2+\mathrm{i}(1+(-1)^n)\pi/2}, \quad (4)$$

$$x_n=r\cos\theta_n,\quad y_n=r\sin\theta_n,\quad \theta_n=\frac{n\pi}{2}+\theta, \quad (5)$$

where x_n and y_n represent the locations of incident beams, θ is the angle between the orientation of the quadruple-like beam and the vertical axes of the lattice, and $|A|^2=1$ is the peak intensity of the probe beam. In our simulation, the lattice intensity $I_{\mathrm{g}}=1.0$ is selected; thus, the real probe-to-lattice beam peak intensity ratio is about 1:4. For the quadruple-like beam, two tails are in phase in diagonal and out of phase with nearest ones. To generate single-site excitation, the parameter $r=0.2d$ is used. By solving Eq. (1) using the split-up beam propagation method, the propagation process can be numerically simulated. Figure 2 shows typical results for two fundamentally excited modes, vertical and diagonal excitation, representing $\theta=0$ and $\theta=\pi/4$, respectively. Under the condition of self-focusing nonlinearity with a biased field $E_0=600$ V/mm ($\gamma=13$), the incident quadruple-like beam can self-trap into localized quadruple modes (Figs. 2(c) and (g)), exiting the lattice with an intensity structure similar to that of the input. Under linear conditions ($\zeta=0$), the input quadruple-like beam experiences discrete diffraction in the square lattice, exiting at $z=60$ of propagation with the intensity structure depicted in Figs. 2(b) and (f) (the transverse zone is two times larger than that in other figures). The results clearly show preferential transport along the lattice axes and that the diffraction tails have three intensity peaks at each lattice site when $\theta=0$, which matches the Bloch mode at point X of the third band, as shown in Fig. 1(c). However, when $\theta=\pi/4$, the output mode

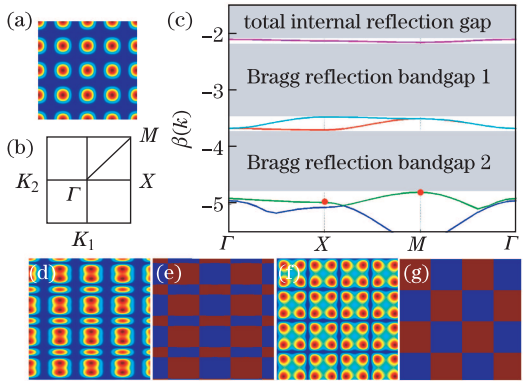

Fig. 1. (Color online) Top row: (a) refractive index of a square lattice; (b) the corresponding first Brillouin zone with high-symmetry points; (c) calculated band gap dispersion relation $\beta(\mathbf{k})$ for $I_{\mathrm{g}}=1.50$, $\gamma=6.00$. Bottom row: bloch modes of high-symmetry points corresponding to the marked red dots in (c). (d, e) and (f, g) show the intensity and phase structure of X and M in the third band, respectively. The blue color of the phase distribution corresponds to the zero phase, while the red color corresponds to the π phase.

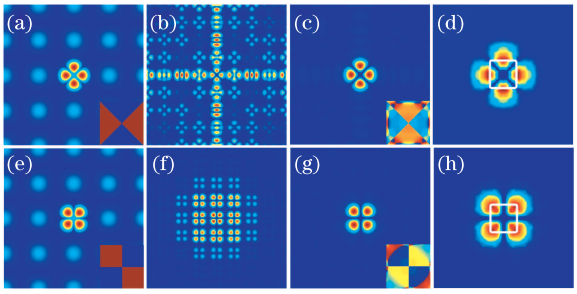

Fig. 2. (Color online) Simulated propagation of two fundamental incident modes: $\theta=0$ (upper row) and $\theta=\pi/4$ (bottom row). (a), (e) Intensity of the input beam with the lattice in the background (the real quadruple-to-lattice beam peak intensity ratio is about 1:4); (b), (f) linear diffraction (nonlinearity off) after 60 mm of propagation in twice as large a space; (c), (g) nonlinear output quadruple localized mode for $E_0=600$ V/mm; (d), (h) the corresponding Fourier spectrum. The white square marks the Brillouin zone. In all figures, the inset shows the corresponding phase structure.

(Fig. 2(f)) shows the characteristics of the Bloch mode at point M of the third band. According to the solitary-wave structure bifurcated from edges of Bloch bands[28], localized quadruple states can be seen as localized waves bifurcating from the third band edge close to points X and M. Fourier spectra (Figs. 2(d) and (h)) of the two localized states also reveal that they are high band gap localized states close to the high-symmetry points X and M. Output modes at other locations are also considered; the same output pattern is obtained and the localized quadruple states are very well preserved during propagation. In summary, high band gap localized quadruple modes close to different high-symmetry points X and M of the third band can be excited under appropriate self-focusing nonlinearity.

Next, the quadruple-like beam is inputted with other orientations and all other parameters are left unchanged. We then consider the case of $\theta = 8°$ (Fig. 3(a)). The nonlinear output pattern (Fig. 3(c)) reveals that the quadruple-like beam can still trap itself into a localized state, but its orientation changes and its intensity tends to distribute into a ring, which is more apparent in Figs. 4(d) and (f). Figure 3(b) depicts the corresponding linear output, wherein the diffraction tails have three intensity peaks at each lattice site along the principal axes of the lattice, resembling the character of the Bloch mode at point X of the third band. Along the lattice diagonal axes, the diffraction tails have four intensity peaks at each lattice site, resembling the character of the Bloch mode at point M of the third band. The Fourier spectrum obtained (Fig. 3(d)) also shows that the spatial spectrum is rotated because of the change in initial orientation.

To explore the dynamics of such a special rotation in detail, the propagation of the quadruple localized mode over a longer distance is investigated. The results of beam propagation simulated up to $z = 80$ (Fig. 4(b)) clearly demonstrate that the input localized state experiences periodic oscillation during propagation. By analyzing the output states at different locations, the localized mode appears to oscillate around the diagonal axis ($\theta = \pi/4$) of the lattice. Figures 4(c)–(f) depict the output intensities and phase structures corresponding to propagation lengths of 43, 55, 66, and 77, respectively, where the four dashed lines in Fig. 4(b) are located. Figures 4(c) and 4(e) show quadruple states in which the oscillation begins to reverse and the degree of oscillation reaches a maximum. The output state at $z = 43$ is similar to the input state, after which it rotates clockwise. Nevertheless, the intensity and phase structure at $z = 55$ illustrate that the quadruple localized state develops into a DCV with a 4π helical phase structure ($m = 2$) around the singular point. The DCV continues to rotate clockwise and break into a quadruple localized structure until it reaches $z = 66$ (Fig. 4(e)). The angle between the orientation of the quadruple localized state and the horizontal direction is close to the incident orientation angle θ. Thereafter, the quadruple state rotates counterclockwise, and a DCV with opposite charge $m = -2$, indicating charge flipping, appears. In summary, the intensity and phase distribution of the localized state varies during propagation, as exhibited by the periodic appearance of a quadruple structure, an $m = 2$ vortex, a quadruple structure,

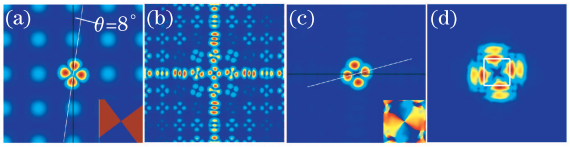

Fig. 3. (Color online) Simulated propagation for $\theta = 8°$. (a) Intensity of the quadruple-like beam; (b) linear diffraction (nonlinearity off) after 60 mm of propagation in twice as large a space; (c) nonlinear output quadruple localized mode and (d) its corresponding Fourier spectrum.

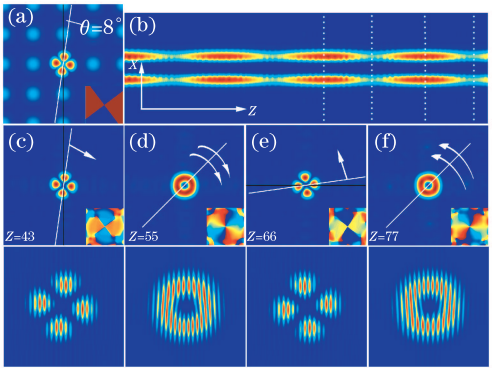

Fig. 4. (Color online) Oscillation of the localized quadruple mode for $\theta = 8°$. Top row: (a) lattice pattern with the waveguide excited by the quadruple-like beam in a single site; (b) side-view of propagation to $z = 80$. Middle row: (c)–(f) nonlinear output intensity corresponding to the location of white dashed lines in (b) with the phase structure inset; from (c) to (f), $z = 43$, 55, 66, and 77, respectively, Bottom row: corresponding interferograms with a tilted plane wave.

and a $m = -2$ vortex. To verify the phase structure, interferograms with a tilted plane wave of the output modes are shown in the bottom row of Fig. 4, which reveals that two humps in diagonal remain in phase for quadruple localized states (Figs. 4(c) and (e)). Topological charges in the vortices are reversed when the oscillation direction is reversed (Figs. 4(d) and (f)).

When other cases for different θ are considered, the results indicate that the quadruple structure tends to oscillate around the diagonal axis and evolve into DCVs during propagation, except for cases of vertical and diagonal excitation. Analysis of the period of the oscillation shows that the rate of oscillation becomes slower and, as a result, the oscillation period becomes longer when the orientation of the incident beam approaches the vertical axis ($\theta = 0$) of the lattice. Our results are comparable with the work of Bartal *et al.*[29], who described second-band single-charged vortex solitons in 2D photonic lattices. Such solitons can be viewed as a coherent superposition of two degenerate modes associated with the second band point X with the same propagation constant. In our simulation, the novel oscillation and appearance of DCV states with periodically flipping vorticity arise from the superposition of two eigenmodes belonging to different high-symmetry points X and M of the third band. Considering different propagation constants, their phase difference changes periodically along the distance of propagation, resulting in the periodic appearance of vortices and charge flipping.

In conclusion, the self-trapping and oscillation of high

band gap quadruple localized modes in 2D optically induced square photonic lattices are studied theoretically. Bloch modes belonging to different high-symmetry points in the high band are excited by excitation of a quadruple-like beam in a single site. The quadruple-like beam can become self-trapped into localized modes by an appropriate self-focusing nonlinearity. Such a special localized state can evolve into DCVs and undergo periodic charge-flipping during propagation solely by changing the orientation relative to the photonic lattices. These results can be useful for theoretical or experimental studies on quadruple beams and vortices in other photonic lattices and discrete nonlinear systems.

This work was supported by the National "973" Program of China (Nos. 2013CB632703 and 2013CB328702), the National Natural Science Foundation of China (Nos. 60908002 and 10904078), the International S&T Cooperation Program of China (No. 2011DFA52870), the Specialized Research Fund for the Doctoral Program of Higher Education (No. 20120031120031), the International Cooperation Program of Tianjin (No. 11ZGHHZ01000), the "111" Project (No. B07013), and the Program for New Century Excellent Talents in University (No. NCET-10-0507).

References

1. D. N. Christodoulides, F. Lederer, and Y. Silberberg, Nature **424,** 817 (2003).
2. T. Schwartz, G. Bartal, S. Fishman, and M. Segev, Nature **446,** 52 (2007).
3. H. Trompeter, W. Krolikowski, D. N. Neshev, A. S. Desyatnikov, A. A. Sukhorukov, Y. S. Kivshar, T. Pertsch, U. Peschel, and F. Lederer, Phys. Rev. Lett. **96,** 053903 (2006).
4. Y. Hu, R. Egger, P. Zhang, X. S. Wang, and Z. G. Chen, Opt. Express **18,** 14679 (2010).
5. P. Zhang, S. Liu, C. B. Lou, F. J. Xiao, X. S. Wang, J. L. Zhao, J. J. Xu, and Z. G. Chen, Phys. Rev. A **81,** 041801(R) (2010).
6. P. Zhang, R. Egger, and Z. G. Chen, Opt. Express **17,** 13151 (2009).
7. P. Zhang, N. K. Efremidis, A. Miller, Y. Hu, and Z. G. Chen, Opt. Lett. **35,** 3252 (2010).
8. D. Mandelik, H. S. Eisenberg, and Y. Silberberg, Phys. Rev. Lett. **90,** 053902 (2003).
9. J. W. Fleischer, M. Segev, N. K. Efremidis, and D. N. Christodoulides, Nature **422,** 147 (2003).
10. J. K. Yang, I. Makasyuk, A. Bezryadina, and Z. G. Chen, Opt. Lett. **29,** 1662 (2004).
11. L. Q. Tang, C. B. Lou, X. S. Wang, D. H. Song, X. Y. Chen, J. J. Xu, Z. G. Chen, H. Susanto, K. Law, and P. G. Kevrekidis, Opt. Lett. **32,** 3011 (2007).
12. D. Neshev, E. Ostrovskaya, Y. Kivshar, and W. Krolikowski, Opt. Lett. **28,** 710 (2003).
13. J. K. Yang, I. Makasyuk, A. Bezryadina, and Z. G. Chen, Stud. Appl. Math. **113,** 389 (2004).
14. J. W. Fleischer, G. Bartal, O. Cohen, O. Manela, M. Segev, J. Hudock, and D. N. Christodoulides, Phys. Rev. Lett. **92,** 123904 (2004).
15. D. N. Neshev, T. J. Alexander, E. A. Ostrovskaya, Y. S. Kivshar, H. Martin, I. Makasyuk, and Z. G. Chen, Phys. Rev. Lett. **92,** 123903 (2004).
16. D. H. Song, C. B. Lou, K. J. H. Law, L. Q. Tang, Z. Y. Ye, P. G. Kevrekidis, J. J. Xu, and Z. G. Chen, Opt. Express **18,** 5873 (2010).
17. E. A. Ostrovskaya and Y. S. Kivshar, Phys. Rev. Lett. **93,** 160405 (2004).
18. X. S. Wang, Z. G. Chen, J. D. Wang, and J. K. Yang, Phys. Rev. Lett. **99,** 243901 (2007).
19. Z. Song, S. Liu, X. Gan, J. Zhao, and E. Li, Chin. Opt. Lett. **9,** 070801 (2011).
20. K. Zhou, Z. Guo, and S. Liu, Chin. Opt. Lett. **8,** 791 (2010).
21. X. S. Wang, Z. G. Chen, and P. G. Kevrekidis, Phys. Rev. Lett. **96,** 083904 (2006).
22. A. Bezryadina, E. Eugenieva, and Z. G. Chen, Opt. Express **31,** 2456 (2006).
23. X. S. Wang, L. Daniel, Z. G. Chen, J. D. Wang, and J. K. Yang, in *Proceedings of Frontiers in Optics* (*FiO*) FThD5 (2008).
24. D. Träger, R. Fischer, D. N. Neshev, A. A. Sukhorukov, C. Denz, W. Królikowski, and Y. S. Kivshar, Opt. Express **14,** 1913 (2006).
25. H. Martin, E. D. Eugenieva, Z. G. Chen, and D. N. Christodoulides, Phys. Rev. Lett. **92,** 123902 (2004).
26. Y. Hu, C. B. Lou, P. Zhang, J. J. Xu, J. K. Yang, and Z. G. Chen, Opt. Lett. **34,** 3259 (2009).
27. A. Bezryadina, D. N. Neshev, A. S. Desyatnikov, J. Young, Z. G. Chen, and Y. S. Kivshar, Opt. Express **14,** 8317 (2006).
28. Z. Q. Shi and J. K. Yang, Phys. Rev. E **75,** 056602 (2007).
29. G. Bartal, O. Manela, O. Cohen, J. W. Fleischer, and M. Segev, Phys. Rev. Lett. **95,** 053904 (2005).